catalysts

MDPI

Article

Scalable Preparation of High-Performance Sludge Biochar with Magnetic for Acid Red G Degradation by Activating Peroxymonosulfate

Feiya Xu [1], Yajun Ji [2,*], Lu Yu [2], Mengjie Ma [2], Dingcan Ma [2] and Junguo Wei [2]

[1] Analysis & Testing Center, Xinyang Normal University, Xinyang 464000, China; Xufy1104@163.com
[2] School of Geographic Sciences, Xinyang Normal University, Xinyang 464000, China; luyu_yl@163.com (L.Y.); mamengjie0308@163.com (M.M.); mdc040903@163.com (D.M.); weijg0102@163.com (J.W.)
* Correspondence: jiyajun928@163.com

Abstract

The sludge pyrolysis technology for biochar production delivers dual environmental benefits, addressing both sludge disposal challenges and enabling environmental remediation through the utilization of the resultant biochar. However, the complex multi-step procedures and low catalyst output in previous studies constrain the practical implementation of this technology. A facile sludge pyrolysis method was constructed to achieve the batch production of municipal sludge biochar (MSB) in this study. Compared to municipal sludge (MS), the resultant MSB showed a higher BET surface area, more well-developed pore channel architecture, and plentiful active sites for activating peroxymonosulfate (PMS). Under the optimized conditions (C_{MSB} = C_{PMS} = 0.2 g/L), 93.34% of Acid Red G (ARG, 20 mg/L) was degraded after 10 min, posing an excellent rate constant of 0.278 min^{-1}. Additionally, MSB demonstrated excellent broad pH adaptability, ion interference resistance, reusability, and recyclability for ARG elimination. It was primary Fe sites that excited PMS to generate $O_2^{\bullet-}$ and Fe-oxo species (Fe^{IV}=O) for ARG degradation. The reaction process exhibited minimal heavy metal leaching, indicating limited environmental risk. Therefore, the practical applicability of the sludge biochar production, coupled with its scalable manufacturing capacity and exceptional catalytic activity, collectively demonstrated that this study established a viable pyrolysis methodology for municipal sludge, offering critical insights for sludge disposal and resource reutilization.

Keywords: sludge; pyrolysis; sludge biochar; organic contaminant; degradation

check for updates

Academic Editor: Vincenzo Vaiano

Received: 9 May 2025
Revised: 25 June 2025
Accepted: 27 June 2025
Published: 30 June 2025

Citation: Xu, F.; Ji, Y.; Yu, L.; Ma, M.; Ma, D.; Wei, J. Scalable Preparation of High-Performance Sludge Biochar with Magnetic for Acid Red G Degradation by Activating Peroxymonosulfate. *Catalysts* **2025**, *15*, 637. https://doi.org/10.3390/catal15070637

Copyright: © 2025 by the authors. Licensee MDPI, Basel, Switzerland. This article is an open access article distributed under the terms and conditions of the Creative Commons Attribution (CC BY) license (https://creativecommons.org/licenses/by/4.0/).

1. Introduction

The acceleration of urbanization has led to the substantial generation of municipal sludge. In 2021, the amount of sludge with 80% moisture content exceeded 60 million tons in China [1,2]. It contains significant concentrations of pathogenic microorganisms and toxic substances. Such sludge necessitates the implementation of effective treatment to mitigate environmental and public health risks [3]. Among the sludge treatment methods, sludge pyrolysis technology can not only achieve effective sludge treatment, but its pyrolysis products can also be utilized for environmental pollution remediation [4–6].

Municipal sludge inherently contains abundant transition metals, carbon, and nitrogen components. After undergoing pyrolysis, they may transform to numerous catalytic sites, thereby granting sludge biochar outstanding advanced oxidation performance [7,8]. The Fe-doped biochar synthesized with biochemical sludge and Fenton sludge exhibited

excellent PMS activation capability, producing reactive oxygen species ($SO_4^{\bullet-}$, ·OH and $^1O_2$) that efficiently degraded organic contaminants [9]. N-doped sludge biochar was synthesized by pyrolyzing sludge at 800 °C under N_2 atmosphere. It exhibited excellent adsorption and persulfate activation performance. 2,4-dichlorophenol (100 mg/L) can be entirely removed in a sludge biochar/persulfate system after 120 min [10]. Seven widely applied fluoroquinolone antibiotics could be effectively removed in an N-doped sludge biochar/PDS system, with rate constants from 0.131 to 0.505 min^{-1} [11]. In the paper sludge biochar/PMS system, the removal efficiency of 4-chlorophenols (20 mg/L) can achieve 100% within 60 min [7]. Numerous studies have demonstrated that employing sludge for biochar synthesis not only achieves waste valorization but also enables the resultant biochar to activate PMS for organic contaminant degradation [12–15].

Most existing studies, however, exhibited notable limitations that hinder their scalability for industrial sludge biochar production. A critical barrier lies in the prevalent requirement for sludge treatment under inert atmospheres (e.g., N_2 or Ar), which is either impractical or significantly increases processing costs in practical operations. Moreover, the synthesis protocols frequently necessitate complex multi-step procedures to achieve highly active biochar, inevitably elevating manufacturing expenses. For example, Wang et al. obtained highly active sludge-derived biochar through a series of steps including drying, grinding, pyrolysis, acid washing, co-impregnation with iron salts and nitrogen sources, and secondary pyrolysis [16]. Although cobalt oxide-loaded sludge biochar demonstrated excellent performance in activating PMS for TC degradation, the synthesis protocol involved consecutive hydrothermal treatment followed by pyrolysis [17]. Similarly, the $CoFe_2O_4$/sludge biochar obtained through intricate pyrolysis–hydrothermal treatment exhibited superior advanced oxidation performance compared to unmodified sludge biochar, achieving 90% TC degradation within 5 min [18]. In addition, the conventional preparation method involves placing several grams of dried sludge in a tube furnace, followed by pyrolysis at elevated temperatures under inert atmosphere to produce a small quantity of sludge biochar [7,19]. From an engineering perspective, the typically low catalyst output fundamentally restricted practical applicability, offering limited guidance for industrial processes. Consequently, this study developed a facile pyrolysis strategy to achieve scalable sludge biochar production by simulating the semi-confined configuration of industrial thermal reactors. The capacity of sludge biochar in PMS activation towards organic pollutant elimination was systematically studied to assess the viability of sludge utilization, aiming to establish fundamental technical references for sludge management technology.

2. Results and Discussion

2.1. Characterization of MSB

The SEM images of MS and MSB are displayed in Figure 1. MS exhibited a dense and compact block-like structure. After pyrolysis, the blocky structure was disrupted, forming more voids and pores. This transformation may lead to a more developed porous structure and a larger BET surface area. The N_2 adsorption/desorption isotherms of MS and MSB are displayed in Figure 2a. Both MS and MSB showed H4-type hysteresis loops and type IV isotherms, implying that they contained abundant mesopores [20,21]. The pore size distribution curves visually indicated that the pore channels in MS and MSB were predominantly mesoporous (Figure 2b). Notably, MSB exhibited a larger specific surface area and pore volume than MS (Table 1), which provided favorable conditions for the active sites within the channels to activate PMS and degrade contaminants.

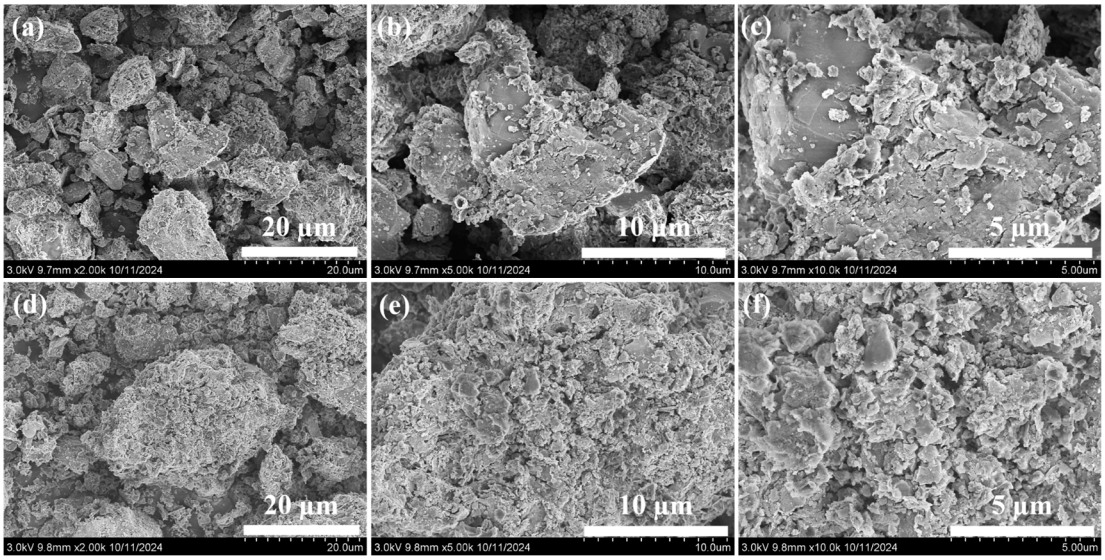


Figure 1. SEM images of MS (**a**–**c**) and MSB (**d**–**f**).

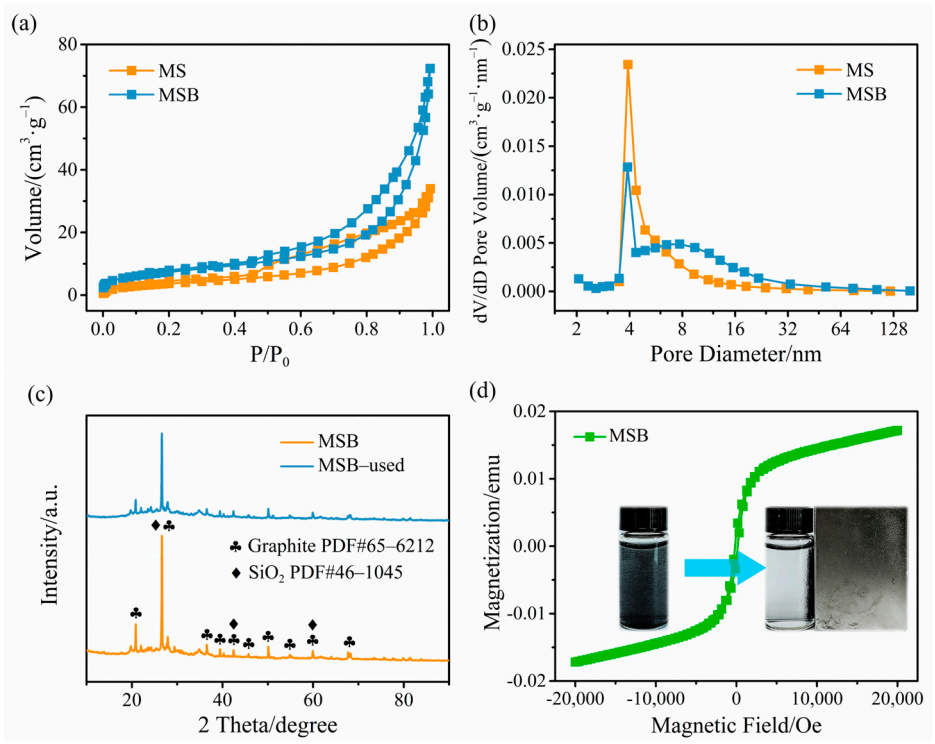


Figure 2. N_2 adsorption/desorption isotherms (**a**) and pore size distribution (**b**) of MS and MSB; XRD patterns (**c**) and magnetization loop (**d**) of MSB.

Table 1. Texture properties of MS and MSB.

Sample	S_{BET} [a]/(m^2/g)	S_{exter} [b]/(m^2/g)	V_{total} [c]/(cm^3/g)	V_{micro} [d]/(cm^3/g)	V_{meso} [e]/(cm^3/g)	D [f]/nm
MS	14.19	18.03	0.036	0	0.036	10.11
MSB	27.04	27.97	0.067	0	0.067	9.93

[a] BET surface area; [b] external surface area; [c] total pore volume; [d] micropore volume; [e] mesopore volume; [f] average pore radius.

The chemical compositions of MS and MSB are presented in Table 2. It was revealed that the primary constituents of both MS and MSB were C, O, Si, and Al. Additionally, they also contained multiple metals, including Fe, Cu, Mn, and Co. When compared to the par-

ent sludge, MSB exhibited higher concentrations of most metallic elements. The abundant transition metals were beneficial to activate PMS towards contaminant elimination. According to the XRD pattern of MSB in Figure 2c, crystalline phases of graphite (PDF#65-6212) were detected instead of the typical broad diffraction peaks associated with amorphous carbon. It indicated that the sludge-derived biochar possessed excellent electronic properties and demonstrated a remarkable degree of graphitization [22,23]. Moreover, MSB displayed a series of characteristic peaks of SiO_2 (PDF#46-1045), with no characteristic peaks from other substances observed. Similar to soil, Si was the main component of MSB, so it exhibited SiO_2 crystal structure. The concentrations of other elements were relatively low, resulting in the absence of other crystal structures.

Table 2. Chemical compositions of MS, MSB, and MSB-used.

Sample	K	O	C	Si	Al	N	Fe	Mg	P	Ca	Na	Cu	Ni	Co	Mn	V	Cr	Zn	As	Cd	Hg	Pb
MS [a]	0.94	-	-	7.92	4.62	-	5.31	0.39	-	0.14	0.087	0.007	ND	0.001	0.077	0.007	0.010	0.069	0.005	0.0001	0.0002	0.005
MSB [a]	1.34	-	-	9.05	6.09	-	7.94	0.46	-	0.20	0.12	0.010	0.005	0.001	0.13	0.010	0.014	0.097	0.006	0.001	0.0003	0.007
MS [b]	0.12	39.89	40.11	5.57	4.50	4.56	1.41	0.43	1.67	1.09	0.27	0.05	0.04	0.24	0.06	ND	ND	ND	ND	ND	ND	ND
MSB [b]	0.32	36.68	39.09	7.77	6.07	4.52	1.67	0.74	1.09	1.31	0.26	0.08	0.05	0.21	0.14	ND	ND	ND	ND	ND	ND	ND
MSB-used [b]	0	32.18	52.23	4.92	3.92	2.82	1.09	0.66	1.08	0.67	0	0.06	0.04	0.20	0.13	ND	ND	ND	ND	ND	ND	ND

[a] Determined by ICP-MS, wt.%; [b] determined by XPS, atomic%; ND: not detected or below detection limit.

The magnetic properties of MSB were determined and are shown in Figure 2d. The distinct magnetization loop observed in MSB indicated its ferromagnetic behavior [24,25]. Elemental composition analysis revealed substantial transition metal content within MS. During pyrolysis, multivalent Fe/Co species were likely to generate, thereby imparting magnetic properties to MSB. Consequently, MSB can be conveniently separated from the solution with a magnet, addressing the poor solid–liquid separation efficiency typically associated with conventional powdered materials.

Figure 3 depicts the XPS spectra of MSB. The surface of MSB was predominantly composed of C and O. Additionally, it contained a diverse array of metallic and non-metallic elements (Table 2 and Figure 3a). Notably, transition metals (Fe, Cu, Co, and Mn) were active for PMS activation to form reactive substances [26–28], consequently enabling the elimination of organic contaminants. The O 1s spectra (Figure 3b) can be divided into three peaks, which were assigned to Fe-O, C-O, and C=O, respectively [29]. Previous studies revealed that $^1O_2$ can be formed through the nucleophilic addition reaction between C=O and PMS [30]. Fe-O was also active to excite PMS to form reactive substances. In the N 1s spectra (Figure 3c), graphitic N, pyrrolic N, Fe-N_x, and pyridinic N were included in MSB. Among them, graphitic N could improve the excitation efficiency of PMS through adjusting the electronic properties of catalysts [31]. Additionally, the activation of PMS can be facilitated due to the strong affinity between Fe-N_x and PMS [32]. From the Fe 2p spectra (Figure 3d), both Fe $2p^{3/2}$ and Fe $2p^{1/2}$ can be deconvoluted into three sub-peaks, corresponding to Fe^{2+}, Fe^{3+}, and satellite peaks, respectively. The Fe species with different valence states can not only effectively activate PMS but also confer magnetic properties to MSB, which has been confirmed in a magnetic test of MSB.

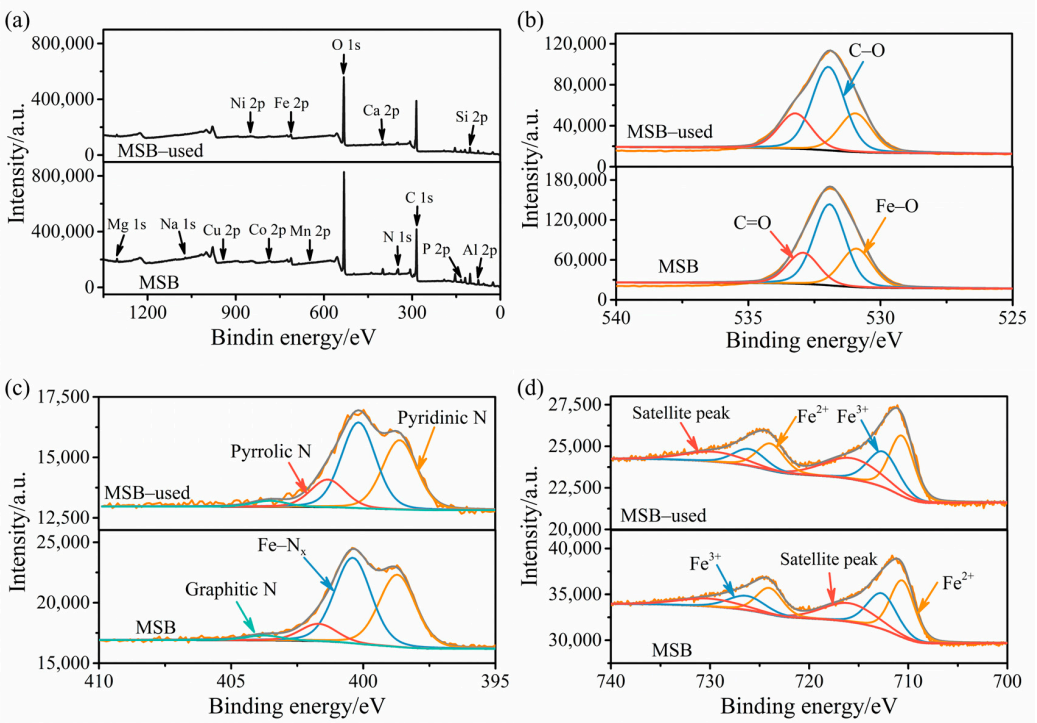


Figure 3. XPS survey spectra (**a**), high-resolution spectra for O 1s (**b**), N 1s (**c**), and Fe 2p (**d**) of MSB and MSB-used.

2.2. Catalytic Degradation Results

Figure 4 displays the elimination of ARG in various systems. With only PMS or MSB, the removal efficiencies of ARG were just 3.91% and 4.31%, respectively (Figure 4a). This implied that it was ineffective to remove ARG solely through the oxidative capability of PMS or the adsorption of MSB. Moreover, the removal efficiency was only 9.06% in the MS/PMS system, implying that the untreated MS had difficulty activating PMS for ARG elimination. Meanwhile, in the MSB/PMS system, about 93.34% of ARG was eliminated after 10 min. The value of the rate constant (k) achieved 0.278 min^{-1}, which was 69.50, 53.46, and 33.90 times higher than that in PMS, MSB, and MS/PMS systems, respectively (Figure 4b). Additionally, the removal efficiency and rate constant were outstanding when compared to other sludge-based biochars reported in the references (Table 3). Therefore, it demonstrated that the obtained MSB exhibited high efficiency in PMS activation towards ARG degradation. The MSB and PMS dosages were optimized and are shown in Figure 4c,d, respectively. When the MSB or PMS concentration was below 0.2 g/L, the elimination of ARG could be facilitated with higher MSB or PMS dosages. However, a highly limited improvement in ARG removal efficiency was observed upon further increasing the concentration of MSB or PMS. Considering the overall removal efficiency within 10 min, the optimal dosages of both MSB and PMS were 0.20 g/L.

Table 3. Performance comparison of sludge-based biochar for organic contaminant degradation.

Sample	Reaction Parameters	*t*/min	Removal Efficiency/%	k/min^{-1}	Reference
Sewage sludge biochar	[Catalyst] = 5 g/L, [PS] = 2 mM, T = 25 °C, [2,4-DCP] = 100 mg/L	120	100	0.119	[10]
$CoFe_2O_4$/ sludge biochar	[Catalyst] = 0.5 g/L, [PMS] = 0.977 mM, T = 25 °C, [TC] = 20 mg/L	30	99.8	-	[18]

Table 3. *Cont.*

Sample	Reaction Parameters	*t*/min	Removal Efficiency/%	k/min^{-1}	Reference
Fe-doped sludge biochar	[Catalyst] = 0.1 g/L, [PMS] = 0.05 g/L, T = 25 °C, [TC] = 10 mg/L	30	90.9	0.3619	[9]
Paper mill sludge biochar	[Catalyst] = 0.3 g/L, [PMS] = 0.6 mM, T = 25 °C, [4-CP] = 20 mg/L	60	100	0.1165	[7]
Co_3O_4@sludge biochar	[Catalyst] = 0.1 g/L, [PMS] = 0.975 mM, T = 25 °C, [OFL] = 20 mg/L	10	99	0.4991	[33]
Co_3O_4@sludge biochar	[Catalyst] = 0.2 g/L, [PMS] = 0.5 mM, T = 20 °C, [TC] = 0.1 mM	60	93.2	0.126	[17]
Microplastics coagulated aluminum sludge biochar	[Catalyst] = 0.1 g/L, [PMS] = 0.2 g/L, T = 25 °C, [TC] = 20 mg/L	30	84.7	0.086	[34]
N-Fe co-doped sludge biochar	[Catalyst] = 0.4 g/L, [PDS] = 0.4 g/L, T = 25 °C, [SMX] = 20 mg/L	120	99%	0.0288	[16]
Tannin extract-sludgederived biochar	[Catalyst] = 0.15 g/L, [PDS] = 0.1 g/L, T = 25 °C, [TC] = 20 mg/L	120	90%	0.0178	[23]
MSB	[Catalyst] = 0.2 g/L, [PMS] = 0.2 g/L, T = 25 ± 2 °C, [ARG] = 20 mg/L	10	93.34	0.278	This work

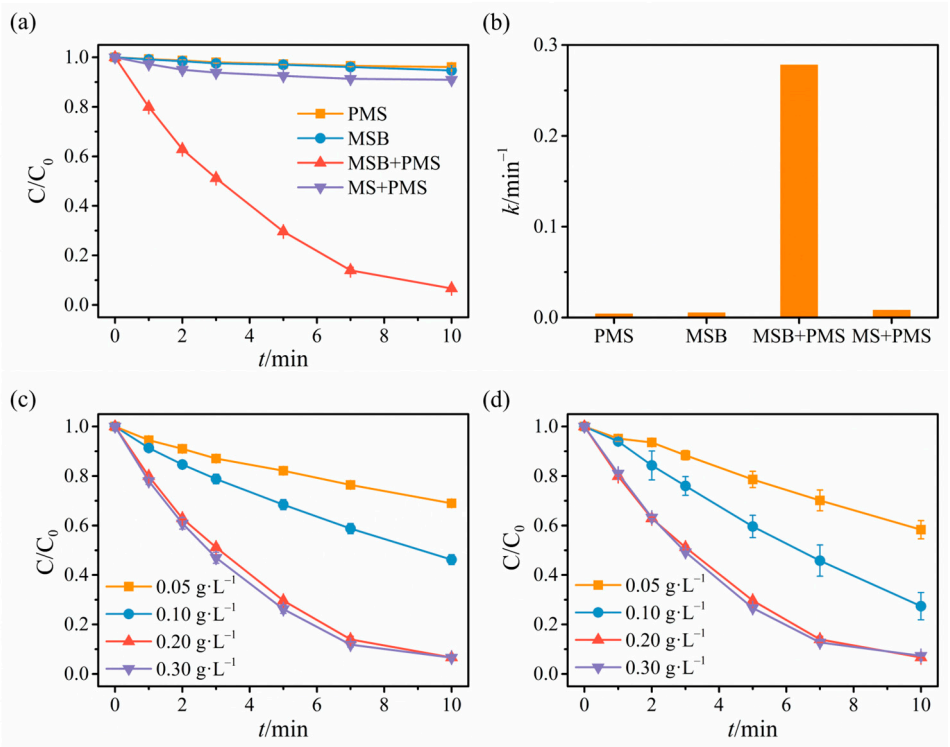


Figure 4. Degradation of ARG. Different systems (**a**); rate constant in different systems (**b**); MSB dosage (**c**); PMS dosage (**d**). (C_{MSB} = C_{PMS} = 0.2 g/L, C_{ARG} = 20 mg/L, T = 25 ± 2 °C).

The influence of solution pH on ARG elimination in the MSB/PMS system is depicted in Figure 5a. When the solution pH was 3–9, over 90% of ARG was eliminated after 10 min, implying that the efficient elimination of ARG in the MSB/PMS system was feasible in a broad pH range. Under extreme alkalinity (pH = 11), the elimination efficiency declined to 20.3%. The rate constant of ARG elimination dramatically reduced to 0.0216 min^{-1} (Figure 5b). This may be attributed to the fact that the electrostatic repulsion between the negatively charged MSB and PMS restrained the excitation of PMS [35].

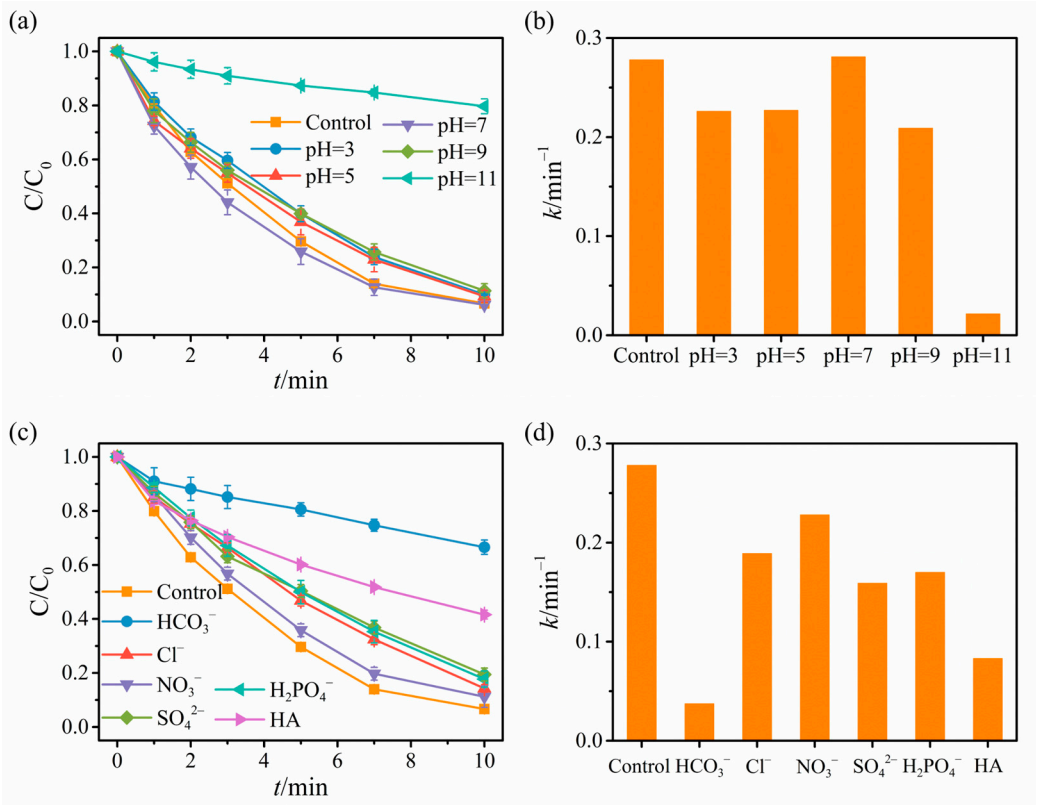


Figure 5. Degradation of ARG under different solution pH values (**a**,**b**) or with co-existing ions and HA (**c**,**d**). (C_{MSB} = C_{PMS} = 0.2 g/L, C_{ARG} = 20 mg/L, T = 25 ± 2 °C).

Figure 5c depicts the influence of co-existing ions and HA on ARG degradation. It was noteworthy that the elimination of ARG was significantly restrained with HCO_3^- and HA. The introduction of HCO_3^- caused the rise in solution pH, which suppressed PMS activation [36]. Additionally, $SO_4^{\bullet -}$ and HO• can be consumed by HCO_3^- (Equations (1) and (2)) [37,38]. As a result, the removal efficiency declined to 33.4%, and the rate constant of ARG elimination dramatically reduced to 0.0373 min^{-1} (Figure 5d), while for HA, it could compete with ARG for reactive substances, leading to a lower elimination efficiency (58.4%) and rate constant (0.083 min^{-1}). In addition, ARG can be efficiently removed even with NO_3^-, Cl^-, $H_2PO_4^-$, or SO_4^{2-}.

$$HCO_3^- + SO_4^{\bullet -} \rightarrow SO_4^{2-} + CO_3^{\bullet -} + H^+ \quad (1)$$

$$HCO_3^- + HO\bullet \rightarrow H_2O + CO_3^{\bullet -} \quad (2)$$

The synthesized MSB was reused for three cycles to assess the reusability. Although the elimination efficiency of ARG gradually decreased with increasing usage cycles, it maintained a relatively high level of 78.5% even after three cycles (Figure 6a), demonstrating an excellent reusability of MSB. After the reaction, the crystal structure was well maintained, exhibiting satisfactory stability (Figure 2c). Additionally, the TOC removal efficiency exceeded 37.6% during the three cycles, implying that partial ARG was thoroughly mineralized.

Considering the presence of diverse heavy metal species in MSB, potential leaching during the reaction may pose secondary environmental hazards. Accordingly, heavy metal concentrations in the post-reaction solution were quantitatively analyzed and are displayed in Figure 7. The primary metal ions were Fe, Zn, Mn, and Ba, with concentrations of 0.24, 0.064, 0.057, and 0.022 mg/L, respectively. The concentrations of other ions were all at trace levels. Therefore, the results substantiated that the MSB-mediated PMS activation system posed negligible heavy metal leaching risks during organic pollutant degradation.

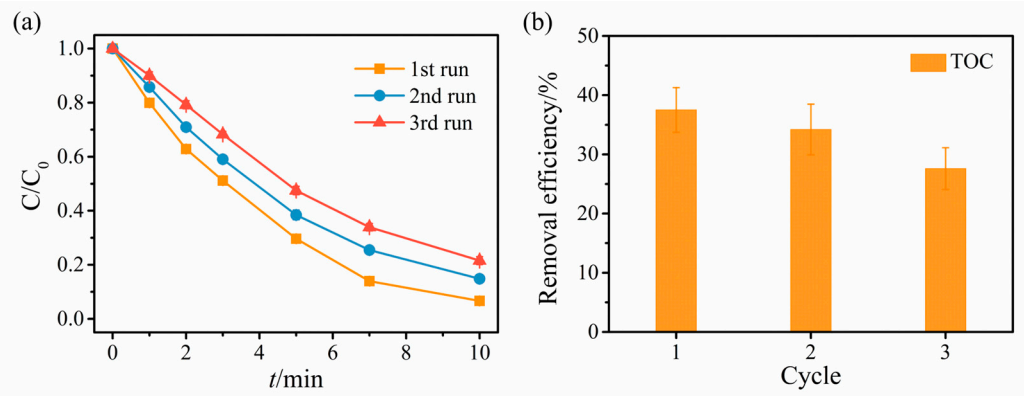


Figure 6. Reusability of MSB for ARG degradation. ARG removal efficiency (**a**); TOC removal efficiency (**b**) (C_{MSB} = C_{PMS} = 0.2 g/L, C_{ARG} = 20 mg/L, T = 25 ± 2 °C).

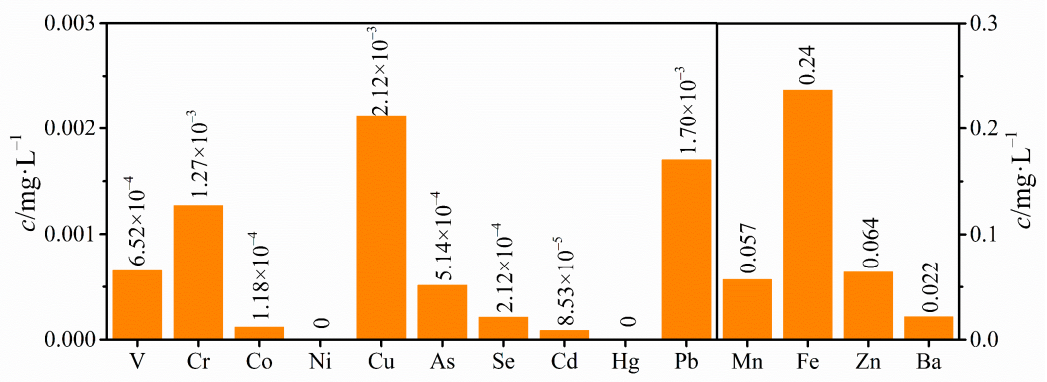


Figure 7. Concentration of leached metal ions in MSB/PMS/ARG system.

2.3. Revelation of Reactive Substances and Catalyst Mechanism

To identify the reactive substances in the MSB/PMS system, a free radical quenching experiment was carried out and is depicted in Figure 8a. SO_4^- and ·OH were scavenged by MeOH, and ·OH was quenched by TBA [39]. However, neither MeOH nor TBA showed a significant influence on ARG removal, implying that ·OH and SO_4^- played insignificant roles in ARG elimination in the MSB/PMS system. Furfuryl alcohol (FFA) was an indicator of $^1O_2$ [40]. With the introduction of FFA, the elimination efficiency and reaction rate slightly reduced to 82.92% and 0.171 min^{-1}, respectively. Given that the depletion of PMS by FFA would also reduce ARG elimination rates [40], it can be concluded that $^1O_2$ exhibited minimal contribution to ARG degradation. *p*-BQ, a widely employed trapping agent for $O_2^{\bullet-}$, was utilized to probe the contribution of $O_2^{\bullet-}$ in the MSB/PMS system [41]. The rate constant of ARG degradation dramatically decreased from 0.278 to 0.0438 min^{-1} with the introduction of 5 mM *p*-BQ (Figure 8b). The higher the concentration of *p*-BQ, the lower the ARG elimination efficiency (Figure 8c). It indicated that $O_2^{\bullet-}$ was to account for the ARG elimination. Additionally, oxalate was applied to passivate the Fe sites [42]. It was noteworthy that the rate constant significantly declined to 0.039 min^{-1} with 5 mM oxalate, and the inhibitory effect demonstrated a positive relationship to the concentration of oxalate, implying that the Fe sites were vital active sites for ARG degradation (Figure 8d). The high-valence Fe-oxo species (Fe^{IV}=O) was common active species in the Fe-based catalyst/PMS system [43]. Fe^{IV}=O can be depleted by DMSO, resulting in a declined elimination efficiency of the pollutant [42]. Thereby, DMSO was applied as an indicator of Fe^{IV}=O [44]. The elimination of ARG was dramatically restrained with the addition of DMSO, implying that Fe^{IV}=O was a vital active species in the MSB/PMS system. Therefore, it was mainly $O_2^{\bullet-}$ and Fe^{IV}=O that were the reactive substances in the MSB/PMS system.

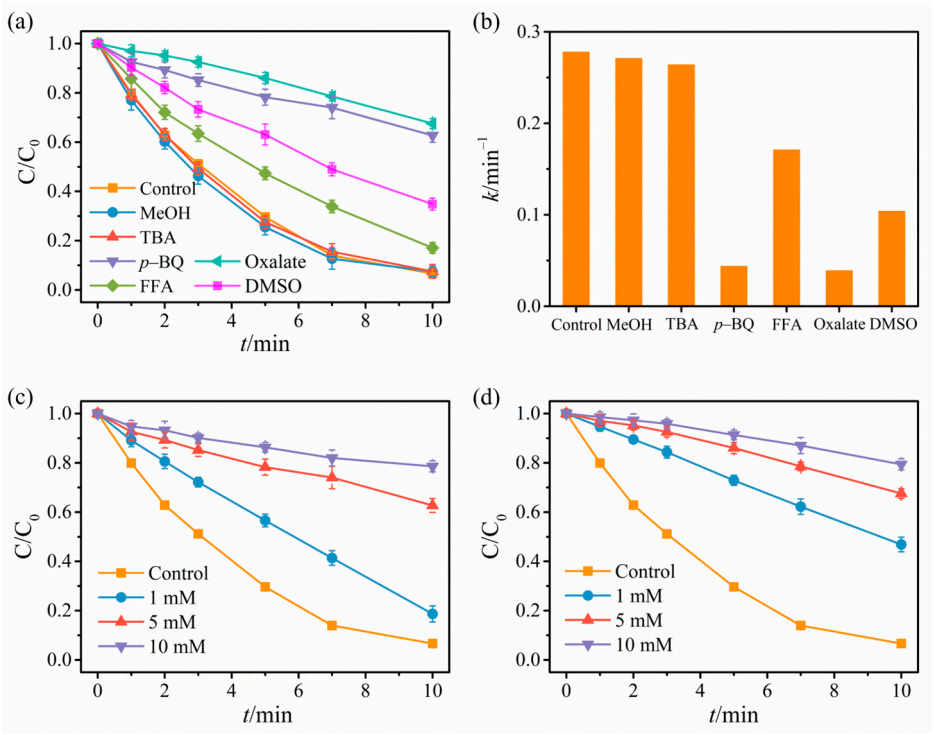


Figure 8. Identification of reactive substances in MSB/PMS system. Free radical quenching experiment (**a**); *k* with different radical quenching agents (**b**); *p*-BQ concentration (**c**); oxalate concentration (**d**) (C_{MSB} = C_{PMS} = 0.2 g/L, C_{ARG} = 20 mg/L, T = 25 ± 2 °C).

The catalytic mechanism was analyzed by investigating the variations in active sites in MSB before and after the reaction. As displayed in Table 4, the ratio of Fe-N_x declined from 47.54% to 44.46%, implying that Fe-N_x might be the active site for PMS excitation. It has been reported that Fe-N_x can be oxidized to Fe^{IV}=O by PMS, which facilitated organic contaminant elimination [43]. Moreover, the contents of Fe-O and Fe^{2+} slightly decreased to 24.54% and 56.70%, respectively. This predominantly resulted from the dissolution of Fe, as well as the excitation of PMS by Fe^{2+} while itself being oxidized to Fe^{3+} during the reaction process. Combined with the analysis results of active species, it can be concluded that Fe-N_x was the predominant active site for PMS excitation towards ARG degradation in the MSB/PMS system. The proposed mechanism of ARG degradation in the MSB/PMS system is depicted in Figure 9.

Table 4. Ratios of different groups in MSB and MSB-used.

Element	Active Group	MSB	MSB-Used
N 1s	Pyridinic N	38.13%	37.74%
	Fe-N_x	47.54%	44.46%
	Pyrrolic N	11.62%	14.84%
	Graphitic N	2.71%	2.96%
O 1s	Fe-O	25.55%	24.54%
	C-O	52.80%	53.01%
	C=O	21.64%	22.45%
Fe 2p	Fe^{2+}	57.54%	56.70%
	Fe^{3+}	42.46%	43.30%

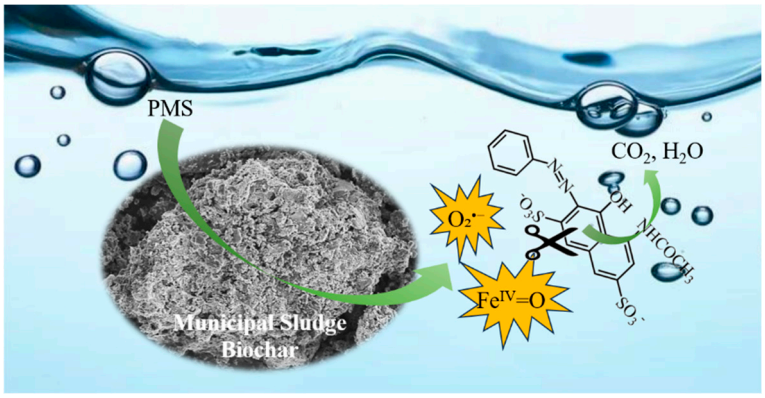


Figure 9. Proposed mechanism of ARG degradation in MSB/PMS system.

3. Experimental Section

3.1. Chemicals

Peroxymonosulfate (PMS), hydrochloric acid (HCl), sodium hydroxide (NaOH), sodium nitrate ($NaNO_3$), sodium sulfate (Na_2SO_4), sodium bicarbonate ($NaHCO_3$), sodium chloride (NaCl), humic acid (HA), methanol (MeOH), tert-butyl alcohol (TBA), furfuryl alcohol (FFA), *p*-benzoquinone (*p*-BQ), dimethyl sulfoxide (DMSO), and sodium oxalate were analytical-grade. They were obtained from Aladdin Biochemical Technology Co., Ltd., Shanghai, China.

3.2. Synthesis of Sludge Biochar

The municipal sludge was collected from a municipal wastewater treatment plant in Xinyang city. Firstly, the obtained municipal sludge was dried at 105 °C overnight. Then, the dried sludge (100 g) was placed into a tubular furnace with the closed inlet gas port and opened outlet gas port. Finally, the sludge was pyrolyzed under 600 °C at a rate of 20 °C/min and held for 0.5 h to acquire municipal sludge biochar (64.86 g). The biochar was ground and sieved with a 200-mesh sieve for subsequent usage. The municipal sludge and synthesized municipal sludge biochar were abbreviated as MS and MSB, respectively.

3.3. Characterization

The morphology of MS and MSB was determined on a scanning electron microscope (S4800, Hitachi, Japan). The crystal structure of MSB was detected on an X-ray diffractometer (SmartLab, Rigaku, Tokyo, Japan) with a scanning range of 10° to 90° at a scan speed of 10°/min. The texture properties of MS and MSB were detected on the physical adsorption instrument (ASAP 2460, Micromeritics, Norcross, GA, USA) after degassing at 200 °C for 5 h. The chemical states of elements on the surface of MSB were determined by an X-ray photoelectron spectrometer (K-ALPHA, ThermoFisher, Waltham, MA, USA). The obtained data were standardized against the C 1s standard signal position (284.8 eV). A vibrating sample magnetometer (8610 VSM, Lake Shore Cryotronics, Westerville, OH, USA) was applied to investigate the magnetic properties of MSB. MS and MSB were digested using HNO_3/HCl/HF (volume ratio, 3:1:1) at 200 °C, followed by elemental content analysis via ICP-MS (8900, Agilent, Santa Clara, CA, USA).

3.4. Catalytic Degradation of ARG

Typically, MSB (10 mg) was dispersed into ARG solution (20 mg/L, 50 mL), followed by adding PMS (10 mg). At regular intervals, 3 mL of reaction mixture was withdrawn, followed by filtrating with a 0.22 μm syringe filter. The residual ARG concentration was measured by detecting the absorbance at 504 nm with a UV–vis spectrometer (TU-1901,

Persee, Beijing, China). Except for the experiments investigating the influence of solution pH, the solution pH was not regulated in other experiments. The degradation results were fitted with pseudo-first-order kinetic model (Equation (3)) to assess the rate of ARG elimination [45].

$$\ln \frac{C}{C_0} = -kt \quad (3)$$

where C is the concentration of ARG at t min, mg/L; C_0 is the initial concentration of ARG, mg/L; k is the rate constant of the reaction, min^{-1}.

In the control experiments, only MSB or PMS were added to investigate the adsorption properties of MSB and the oxidation capacity of PMS. Moreover, the factors of MSB concentration, PMS concentration, solution pH, co-existing ions, and catalyst reutilization on ARG elimination were comprehensively investigated. The post-reaction solution was directly employed without dilution for ICP-MS analysis to quantify the concentrations of heavy metals leached from MSB.

4. Conclusions

A facile pyrolysis strategy to achieve scalable sludge biochar production was constructed by simulating the semi-confined configuration of industrial thermal reactors. MSB obtained by pyrolyzing the dried sludge at 600 °C exhibited a larger specific surface area and pore volume than MS. It also exhibited ferromagnetism, providing it with desirable solid–liquid separation properties. The prepared MSB exhibited excellent performance for PMS activation towards ARG degradation. Under the optimized reaction conditions (C_{MSB} = C_{PMS} = 0.2 g/L), 93.34% of ARG was eliminated after 10 min, and the rate constant of the reaction achieved 0.278 min^{-1}. MSB showed an outstanding advanced oxidation performance among the sludge-based biochar. Moreover, the MSB/PMS system posed remarkable capability for ARG elimination, even in a wide solution pH range (3–9) or with co-existing ions (NO_3^-, Cl^-, $H_2PO_4^-$, or SO_4^{2-}) and HA. It also showed robust recycling performance. The catalyst mechanism study demonstrated that it was mainly Fe-N_x that activated PMS to generate Fe^{IV}=O for ARG degradation. After pyrolysis, heavy metals were immobilized in MSB, and the concentrations of the leached heavy metals were extremely low, posing minimal environmental risk. Therefore, the reaction conditions for biochar preparation in this study closely resemble those of industrial pyrolysis reactors, providing valuable references for the industrial pyrolysis treatment of sludge.

Author Contributions: F.X.: methodology, resources, supervision, and writing—original draft. Y.J.: conceptualization, funding acquisition, and writing—review and editing. L.Y.: data curation. M.M.: investigation. D.M.: data curation. J.W.: investigation. All authors have read and agreed to the published version of the manuscript.

Funding: The authors acknowledged the supporting from Natural Science Foundation of Henan (No. 252300421568) and Science and Technology Department of Henan Province (No. 242102320078).

Data Availability Statement: The original contributions presented in this study are included in the article. Further inquiries can be directed to the corresponding author.

Conflicts of Interest: The authors declare no conflicts of interest.

References

1. Meng, Z.; Xiong, H.; Zhu, C.; Xu, G. Study on the process technology of energy saving and consumption reducing for municipal sludge-based biochar. *Renew. Energ.* **2024**, *220*, 119606. [CrossRef]
2. Zhang, X.; Zhao, B.; Liu, H.; Zhao, Y.; Li, L. Effects of pyrolysis temperature on biochar's characteristics and speciation and environmental risks of heavy metals in sewage sludge biochars. *Environ. Technol. Inno.* **2022**, *26*, 102288. [CrossRef]

3. Liu, X.; Li, Y.; Zhou, H.; Guo, J.; Xiao, Y.; Liu, C.; An, B.; Liang, Z. Phosphate Removal by Ca-Modified Magnetic Sludge Biochar Prepared by a One-Step Hydrothermal Method. *Catalysts.* **2023**, *13*, 927. [CrossRef]
4. Hu, T.; Zhao, S.; Huang, Y.; Chen, Z.; Zhang, X.; Wei, C.; Zeng, S.; Liu, L. Potential removals of tetracycline and sulfamethoxazole by iron-loaded sludge biochar. *J. Water Process Eng.* **2023**, *54*, 103962. [CrossRef]
5. Ihsanullah, I.; Khan, M.T.; Zubair, M.; Bilal, M.; Sajid, M. Removal of pharmaceuticals from water using sewage sludge-derived biochar: A review. *Chemosphere.* **2022**, *289*, 133196. [CrossRef]
6. Liu, Y.; Chen, Z.; Liu, C.; Li, W.; Yao, X.; Tian, T.; Zhao, C.; Tao, S.; Qiao, W.; Zhang, M. Large-Scale Preparation of Granular Sludge@MOF-Derived Hierarchical Porous Carbon Catalysts for Advanced Oxidation Process: Preparation Process and Intrinsic Degradation Mechanism. *Catalysts.* **2025**, *15*, 264. [CrossRef]
7. Liu, J.; Liu, Z.; Miao, R.; Wang, Y.; He, L.; Zhou, H.; Liang, S.; Lei, X.; Deng, X. Sludge-derived biochar applied in peroxymonosulfate (PMS) activation: Regulation of active sites and synergistic production of reaction oxygen species. *J. Taiwan Inst. Chem. Eng.* **2025**, *171*, 106071. [CrossRef]
8. Rangabhashiyam, S.; Lins, P.V.d.S.; Oliveira, L.M.T.d.M.; Sepulveda, P.; Ighalo, J.O.; Rajapaksha, A.U.; Meili, L. Sewage sludge-derived biochar for the adsorptive removal of wastewater pollutants: A critical review. *Environ. Pollut.* **2022**, *293*, 118581. [CrossRef]
9. Lin, L.; Fang, W.; Liang, Q.; Xing, Y.; Sun, M.; Luo, H. Synthesis of Fe-doped sludge biochar from Fenton sludge for efficient activation of peroxymonosulfate in tetracycline hydrochloride degradation. *J. Environ. Chem. Eng.* **2024**, *12*, 112590. [CrossRef]
10. Cui, J.; Wei, L.; Ning, C.; Zhang, F.; Cui, J.; Xiangli, P. Highly-efficient persulfate activation by nitrogen-doped biochar derived from dewatered sewage sludge for 2,4-dichlorophenol removal: Process and mechanism. *J. Environ. Chem. Eng.* **2024**, *12*, 112561. [CrossRef]
11. Fang, Z.; Zhao, S.; Xue, G.; Wang, X.; Sun, P.; Yu, Y.; Zhou, Z.; Wang, Q.; Qian, Y. Enhanced removal of fluoroquinolone antibiotics by peroxydisulfate activated with N-doped sludge biochar: Performance, mechanism and toxicity evaluation. *Sep. Purif. Technol.* **2023**, *305*, 122469. [CrossRef]
12. Zeng, H.; Xu, J.; Li, J.; Chen, Y.; Zou, J.; Liu, N.; Wang, Y.; Hao, R.; Li, D.; Zhang, J. Activation of peroxymonosulfate by sludge-derived magnetic biochar for pollutant removal: Performance, applicability, and synergetic mechanism of iron species and carboxylated biochar. *Chem. Eng. J.* **2024**, *485*, 149744. [CrossRef]
13. Tan, W.; Chen, Y.; Liu, Y.; Pan, H.; Liu, X.; Shi, Q.; Li, Z.; Zhao, C. Periodate activation by a Fenton sludge biochar for enhanced tetracycline degradation: Identification of key factors through machine learning. *Inorg. Chem. Commun.* **2025**, *176*, 114295. [CrossRef]
14. Liu, X.; Luo, F.; Liang, L.; Li, N.; Zhou, Z.; Liu, Y.; Pan, H. Enhanced dewaterability of waste activated sludge via peroxymonosulfate activation process initiated by magnetic biochar derived from iron-rich sludge. *Sustain. Chem. Pharm.* **2024**, *39*, 101585. [CrossRef]
15. Cao, J.; Jiang, Y.; Tan, X.; Li, L.; Cao, S.; Dou, J.; Chen, R.; Hu, X.; Qiu, Z.; Li, M.; et al. Sludge-based biochar preparation: Pyrolysis and co-pyrolysis methods, improvements, and environmental applications. *Fuel.* **2024**, *373*, 132265. [CrossRef]
16. Wang, S.; Meng, X.; Yan, X.; Wang, Y.; Mo, Y.; Chen, Y.; Xu, W.; Shi, W. Iron and nitrogen modified sludge biochar efficiently activated persulfate for mineralization of sulfamethoxazole in groundwater. *J. Environ. Chem. Eng.* **2023**, *11*, 111319. [CrossRef]
17. Shi, Q.; Yang, R.; Liu, M.; Feng, Y.; Li, Z.; Zhu, W. A highly-efficient peroxymonosulfate activator using a sewage sludge derived biochar supported cobalt oxide: Mechanism and characteristics. *Process Saf. Environ. Prot.* **2024**, *192*, 1319–1329. [CrossRef]
18. Huang, N.; Wang, T.; Wu, Y.; Wang, F.; Zhang, D.; Zhou, R.; Kong, C.; Yang, Z.; Zhang, H.; Zhu, H. Preparation of magnetically recyclable hierarchical porous sludge-pine needle derived biochar loaded $CoFe_2O_4$ nanoparticles for rapid degradation of tetracycline by activated PMS. *Mater. Today Commun.* **2023**, *35*, 106313. [CrossRef]
19. Li, S.; Huang, D.; Cheng, M.; Wei, Z.; Du, L.; Wang, G.; Chen, S.; Lei, L.; Chen, Y.; Li, R. Application of sludge biochar nanomaterials in Fenton-like processes: Degradation of organic pollutants, sediment remediation, sludge dewatering. *Chemosphere* **2022**, *307*, 135873. [CrossRef]
20. Ji, Y.; Xie, Y.; Zheng, L.; Xu, F. Efficient activation of peroxymonosulfate by porous Co-doped $LaFeO_3$ for organic pollutants degradation in water. *J. Solid State Chem.* **2021**, *297*, 122077. [CrossRef]
21. Ji, Y.; Zhang, W.; Yang, H.; Ma, F.; Xu, F. Green synthesis of poly(pyrrole methane) for enhanced adsorption of anionic and cationic dyes from aqueous solution. *J. Colloid Interf. Sci.* **2021**, *590*, 396–406. [CrossRef] [PubMed]
22. Wang, H.; Guo, W.; Liu, B.; Si, Q.; Luo, H.; Zhao, Q.; Ren, N. Sludge-derived biochar as efficient persulfate activators: Sulfurization-induced electronic structure modulation and disparate nonradical mechanisms. *Appl. Catal. B Environ.* **2020**, *279*, 119361. [CrossRef]
23. Yang, Y.; Lin, J.; Liu, Z.; Liu, M. Degradation of tetracycline by peroxydisulfate activation on sludge-derived biochar modified with tannin extract. *Process Saf. Environ. Prot.* **2023**, *173*, 472–484. [CrossRef]

24. Ji, Y.; Xu, F.; Zhang, P.; Xu, Y.; Zhang, G. Green synthesis of poly(pyrrole methane)-based adsorbent for efficient removal of chromium(VI) from aqueous solution. *J. Clean. Prod.* **2021**, *293*, 126197. [CrossRef]
25. Ji, Y.; Xu, F.; Fang, K.; Liu, H.; Pan, X.; Jin, Z.; Zheng, L.; Wang, L. Facile synthesis of carbon nitride nanotube confined nano Fe^0 for boosting activation of peroxymonosulfate towards tetracycline removal. *Environ. Technol. Inno.* **2025**, *38*, 104079. [CrossRef]
26. Wang, Z.; Yang, L.; Shan, Z.; Tang, L.; Chen, C.; Lan, Y.; Li, W. Fabrication of magnetic cobalt-iron composite moored on carbon derived from cigarette butts (Co-Fe@CCB) for peroxymonosulfate activation to efficiently degrade Rhodamine B. *J. Water Process Eng.* **2023**, *53*, 103845. [CrossRef]
27. Ma, Y.; Meng, Y.; Wang, Z.; Xin, Y.; Lv, X.; Li, Q.; Wang, H.; Xie, H.; Zhang, Z. In-situ construction of mesoporous $CuCo_2O_4$ decorated CNTs networks as a long-lasting peroxymonosulfate activator for rapid removal of aqueous micropollutants. *Chem. Eng. J.* **2023**, *476*, 146694. [CrossRef]
28. Yang, Z.; Hou, J.; Wu, J.; Miao, L. Mesoporous carbon framework supported Fe-Cu-Mn oxides as an efficient peroxymonosulfate catalyst for the control of harmful algal blooms: Synergism of Fe-Cu-Mn and role of mesoporous carbon. *Chem. Eng. J.* **2023**, *461*, 141877. [CrossRef]
29. Yao, Y.; Lai, L.; Yu, Z.; Pan, Y.; Yu, Y.; Lo, V.; Roy, A.; Chivers, B.; Zhong, X.; Wei, L.; et al. Carbon/iron by-product from catalytic methane decomposition as recyclable Fenton catalyst for pollutant degradation. *J. Hazard. Mater.* **2022**, *437*, 129328. [CrossRef]
30. Zhen, J.; Sun, J.; Xu, X.; Wu, Z.; Song, W.; Ying, Y.; Liang, S.; Miao, L.; Cao, J.; Lv, W.; et al. $M-N_3$ Configuration on Boron Nitride Boosts Singlet Oxygen Generation via Peroxymonosulfate Activation for Selective Oxidation. *Angew. Chem. Int. Edit.* **2024**, *63*, e202402669. [CrossRef]
31. He, Y.L.; He, C.S.; Lai, L.D.; Zhou, P.; Zhang, H.; Li, L.L.; Xiong, Z.K.; Mu, Y.; Pan, Z.C.; Yao, G.; et al. Activating peroxymonosulfate by N and O co-doped porous carbon for efficient BPA degradation: A re-visit to the removal mechanism and the effects of surface unpaired electrons. *Appl. Catal. B Environ.* **2022**, *314*, 121390. [CrossRef]
32. Zhang, B.; Li, X.; Akiyama, K.; Bingham, P.A.; Kubuki, S. Elucidating the Mechanistic Origin of a Spin State-Dependent FeNx-C Catalyst toward Organic Contaminant Oxidation via Peroxymonosulfate Activation. *Environ. Sci. Technol.* **2022**, *56*, 1321–1330. [CrossRef] [PubMed]
33. Liu, Z.; Hu, Y.; Huang, Y.; Zhang, Z.; Lv, Y.; Liu, M. Rapid removal of ofloxacin with peroxymonosulfate activation process mediated by Co_3O_4/Sludge-derived biochar composite: Unveiling the enhancement of biochar. *Sep. Purif. Technol.* **2024**, *342*, 127077. [CrossRef]
34. Yang, M.; Wang, W.; Ma, H.; Chen, L.; Ma, H.; Shi, F. Efficient tetracycline hydrochloride degradation via peroxymonosulfate activation by N doped coagulated sludge based biochar: Insights on the nonradical pathway. *Environ. Res.* **2025**, *266*, 120554. [CrossRef]
35. Wang, Y.; Sun, Y.; Wang, R.; Gao, M.; Xin, Y.; Zhang, G.; Xu, P.; Ma, D. Activation of peroxymonosulfate with cobalt embedded in layered delta-MnO_2 for degradation of dimethyl phthalate: Mechanisms, degradation pathway, and DFT calculation. *J. Hazard. Mater.* **2023**, *451*, 130901. [CrossRef]
36. Pan, S.; Guo, X.; Lu, X.; Li, R.; Hu, H.; Nie, X.; Liu, B.; Chen, R.; Zhu, M.; Hei, S.; et al. Boosting peroxymonosulfate activation by a novel bifunctional core-shell nanoreactor $MnFe_2O_4$@HZO for nitrilotris-methylenephosphonic acid removal. *Appl. Catal. B Environ.* **2023**, *330*, 122508. [CrossRef]
37. Bai, Z.; Wang, S.; Tian, J.; Gao, S.; Zhang, R.; Liu, X. Aluminum-based layered metal oxides activating peroxymonosulfate for bisphenol A degradation via surface-bound sulfate radicals and singlet oxygen. *J. Hazard. Mater.* **2022**, *424*, 127515. [CrossRef]
38. Zhang, Z.; Dai, Y. Co_3O_4/C-PC composite derived from pomelo peel-loaded ZIF-67 for activating peroxymonosulfate (PMS) to degrade ciprofloxacin. *J. Water Process Eng.* **2022**, *49*, 103043. [CrossRef]
39. Huo, J.; Wei, J.; Li, J.; Jiang, Z.; Ji, W.; Wang, L.; Li, Y.; Cui, N.; Guan, S.; Li, J.; et al. Boron amplifies the cation vacancy effect to enhance multi-pathway degradation of organic pollutants. *Appl. Catal. B Environ. Energy* **2025**, *371*, 125278. [CrossRef]
40. Zhou, C.; Guo, Y.; Du, S.; Sui, M. Ultrafast Fenton-like reaction using a peroxymonosulfate-mediated confined-Fe^0 catalyst for the degradation of sulfamethoxazole. *Appl. Catal. B Environ. Energy* **2024**, *358*, 124442. [CrossRef]
41. Luo, X.; You, Y.; Zhong, M.; Zhao, L.; Liu, Y.; Qiu, R.; Huang, Z. Green synthesis of manganese-cobalt-tungsten composite oxides for degradation of doxycycline via efficient activation of peroxymonosulfate. *J. Hazard. Mater.* **2022**, *426*, 127803. [CrossRef] [PubMed]
42. Li, H.; Shan, C.; Pan, B. Fe(III)-Doped g-C_3N_4 Mediated Peroxymonosulfate Activation for Selective Degradation of Phenolic Compounds via High-Valent Iron-Oxo Species. *Environ. Sci. Technol.* **2018**, *52*, 2197–2205. [CrossRef] [PubMed]
43. Cheng, C.; Ren, W.; Miao, F.; Chen, X.; Chen, X.; Zhang, H. Generation of Fe^{IV}=O and its Contribution to Fenton-Like Reactions on a Single-Atom Iron-N-C Catalyst. *Angew. Chem. Int. Edit.* **2023**, *62*, e202218510. [CrossRef] [PubMed]

44. Ji, Y.; Xu, F.; Yan, J.; Liu, X.; Li, X. Constructing carbon nitride embedded Fe^0 for efficient activation of peroxymonosulfate towards organic pollutants degradation in water. *J. Water Process Eng.* **2024**, *68*, 106556. [CrossRef]
45. Huang, G.X.; Wang, C.Y.; Yang, C.W.; Guo, P.C.; Yu, H.Q. Degradation of Bisphenol A by Peroxymonosulfate Catalytically Activated with $Mn_{1.8}Fe_{1.2}O_4$ Nanospheres: Synergism between Mn and Fe. *Environ. Sci. Technol.* **2017**, *51*, 12611–12618. [CrossRef]

Disclaimer/Publisher's Note: The statements, opinions and data contained in all publications are solely those of the individual author(s) and contributor(s) and not of MDPI and/or the editor(s). MDPI and/or the editor(s) disclaim responsibility for any injury to people or property resulting from any ideas, methods, instructions or products referred to in the content.